Check for updates

Temperature-dependent swelling transitions in MXene Ti₃C₂Tₓ†

Artem Iakunkov,[a] Andreas Nordenström, [iD][a] Nicolas Boulanger, [iD][a] Christoph Hennig,[b,c] Igor Baburin[d] and Alexandr V. Talyzin [iD] *[a]

Swelling is a property of hydrophilic layered materials, which enables the penetration of polar solvents into an interlayer space with expansion of the lattice. Here we report an irreversible swelling transition, which occurs in MXenes immersed in excess dimethyl sulfoxide (DMSO) upon heating at 362–370 K with an increase in the interlayer distance by 4.2 Å. The temperature dependence of MXene Ti₃C₂Tₓ swelling in several polar solvents was studied using synchrotron radiation X-ray diffraction. MXenes immersed in excess DMSO showed a step-like increase in the interlayer distance from 17.73 Å at 280 K to 22.34 Å above ~362 K. The phase transformation corresponds to a transition from the MXene structure with one intercalated DMSO layer into a two-layer solvate phase. The transformation is irreversible and the expanded phase remains after cooling back to room temperature. A similar phase transformation was observed also for MXene immersed in a 2 : 1 H₂O : DMSO solvent ratio but at a lower temperature. The structure of MXene in the mixed solvent below 328 K was affected by the interstratification of differently hydrated (H₂O)/solvated (DMSO) layers. Above the temperature of the transformation, the water was expelled from MXene interlayers and the formation of a pure two-layer DMSO–MXene phase was found. No changes in the swelling state were observed for MXenes immersed in DMSO or methanol at temperatures below ambient down to 173 K. Notably, MXenes do not swell in 1-alcohols larger than ethanol at ambient temperature. Changing the interlayer distance of MXenes by simple temperature cycling can be useful in membrane applications, *e.g.* when a larger interlayer distance is required for the penetration of ions and molecules into membranes. Swelling is also very important in electrode materials since it allows penetration of the electrolyte ions into the interlayers of the MXene structure.

1. Introduction

Two-dimensional (2D) materials have been rather actively studied over the past decade in both single layered and multi-layered forms. 2D materials can be both hydrophobic (*e.g.* graphene or boron nitride) and hydrophilic (clays, graphite/graphene oxide and some MXenes[1]). Swelling is a key property of hydrophilic multilayer 2D materials that is crucial in many applications. For example, swelling determines the size of permeation channels in membrane applications,[2,3] the pore size of electrodes inside energy storage devices (*e.g.* supercapacitors)[4] and the sorption properties for the removal of pollutants.[5]

Water and many other polar solvents are known to penetrate easily between individual sheets of hydrophilic 2D materials, expanding the interlayer distance. Saturated swelling is easily achieved by immersing hydrophilic materials into liquid water (or other solvents) or by exposure to saturated vapours.[6–8] Intercalated solvent molecules are relatively weakly bound to 2D sheets by hydrogen bonding and in many cases the swelling is reversible. For example, water easily evaporates from the swelled structures of clays and graphite oxide after the exposure of hydrated materials to air.[9]

The swelling of clays and graphite/graphene oxide has been studied rather extensively over last 100 years, revealing many unusual effects.[10] For example, the swelling of graphite oxide in a variety of solvents (*e.g.* water, alcohols, amines, nitriles, *etc.*) was studied under temperature and pressure variations.[11–16] Solvent molecules can be intercalated into the GO structure, forming one or several layers depending on the solvent nature and specific temperature/pressure conditions.[7,17–21] Temperature- and pressure-driven phase transitions related to the insertion or de-insertion of solvent layers were discovered for Brodie GO (BGO) immersed in

[a]Department of Physics, Umeå University, Umeå, SE-901 87, Sweden. E-mail: alexandr.talyzin@umu.se

[b]Institute of Resource Ecology, Helmholtz Zentrum Dresden Rossendorf, Bautzner Landstrasse 400, 01328 Dresden, Germany

[c]The Rossendorf Beamline, European Synchrotron Radiation Facility, 71 Avenue des Martyrs, 38043 Grenoble, France

[d]Theoretische Chemie, Technische Universität Dresden, 01062 Dresden, Germany

†Electronic supplementary information (ESI) available. See DOI: https://doi.org/10.1039/d2nr03075f

several alcohols, acetonitrile, DMF and some other solvents.[12,14,22–25] Gradual changes in the interlayer distance have been found for BGO and Hummers GO (HGO) as a function of humidity or under temperature variations in a solvent-immersed state.[13,15,26] The gradual changes in the GO structure are commonly explained by random interstratification: random stacking of differently hydrated (or solvated) interlayers.[8,9,26]

Unlike clays and GO that have been known for over a century, 2D MXenes were discovered relatively recently. So far, only a very few focused studies are available on MXenes swelling in polar solvents even under ambient conditions.[27–30] A single study of the swelling of MXene $Ti_3C_2T_x$ under compression and decompression has been reported so far,[31] but systematic studies of temperature-dependent swelling are not yet available.

The most common MXene, $Ti_3C_2T_x$, is also the most studied for its swelling properties. It can be considered as a model material for many other MXenes. Swelling is one of the key properties of MXenes, which helps to delaminate bulk materials on single sheets using, *e.g.* mild sonication, in polar solvents.[32] The swelling of $Ti_3C_2T_x$ depends very strongly on the synthesis method. An original and still most common method to produce $Ti_3C_2T_x$ is to etch Al away from the "MAX phase" using HF.[33] The resulting Ti_3C_2 sheets are terminated by several kinds of functional groups, including fluorine, oxygen and hydroxyls denoted as "T_x". $Ti_3C_2T_x$ produced by this method can be delaminated to produce 2D sheets using dimethyl sulfoxide (DMSO).[34,35] The delamination is enabled by swelling in DMSO, which seems to be one of few solvents capable of intercalating $Ti_3C_2T_x$ prepared by HF etching. This type of MXene does not swell in most common polar solvents like water and alcohols.[34]

However, swelling in water, alcohols and several other solvents has been found for $Ti_3C_2T_x$ prepared by HF + LiCl[1] and LiF + HCl etching procedures. "Clay-like" swelling under ambient conditions was reported for $Ti_3C_2T_x$ synthesized with Li-intercalation or after ion exchange with alkali or alkali-earth cations.[1,27,29,36,37] There are also data suggesting that water is more ordered in swollen ion-intercalated MXenes.[38]

It is important to distinguish between "crystalline" swelling, when the lattice expansion clearly corresponds to the insertion of one or several discrete solvent layers, and osmotic swelling, which is typically rather large and controlled by the charge balance inside interlayers.[39] The swelling of MXenes in pure solvents is typically crystalline but in some case it could also be osmotic, *e.g.* in NaOH solutions with low concentrations.[40] Once again, there are some strong similarities in the swelling of GO[41,42] and MXenes in NaOH solutions.[40]

The surface of a single MXene sheet is terminated, at least partly, by the same types of functional groups (*e.g.* OH groups) as graphene oxide. Therefore, one could possibly expect to find some temperature-dependent swelling effects for $Ti_3C_2T_x$ immersed in liquid polar solvents similar to those found in BGO and HGO. On the other hand, the presence of fluorine-related functional groups in MXenes and the absence of these groups in graphene oxide could result in some significant differences.

Here we report the results of *in situ* temperature-dependence experiments with $Ti_3C_2T_x$ immersed in several common polar solvents performed using synchrotron radiation X-ray diffraction (XRD). No transitions between differently swelled phases were found for $Ti_3C_2T_x$ immersed in water and methanol upon cooling or heating. Moreover, swelling in alcohols larger than ethanol was not found even under ambient conditions. A sharp phase transformation related to the insertion of an additional solvent layer was found for $Ti_3C_2T_x$ immersed in DMSO at temperatures above ambient. The transformation was not reversible and an expanded two-layer DMSO–$Ti_3C_2T_x$ structure remained upon cooling back to room temperature.

2. Materials and methods

$Ti_3C_2T_x$ was synthesized here using two procedures reported previously.[31,36,43,44]

The first method was the synthesis of MXenes using a LiCl + HF etching procedure. The MAX phase Ti_3AlC_2 precursor (Carbon®, Ukraine) was first etched with a mixture of LiCl (99% Sigma Aldrich) and 10% HF (by diluting commercial 48% HF, Sigma Aldrich) for 22 h at 50 °C using a molar ratio of 1 : 5 between the initial MAX phase and LiCl. At the end of the oxidation, the resulting mixture was centrifuged (15 000 rpm for 15 min) and washed with 6 M HCl in order to remove all the Li-salt impurities. The resulting material was placed in a 1 M LiCl solution for 24 h under argon to ensure the intercalation of Li into the final structure.[31] After this, the material was washed using water until a pH value of 6 was achieved. Finally, the water dispersion was centrifuged at 500–1000 rpm for 10 min and only the supernatant was collected and vacuum dried to obtain MXenes. Mild centrifugation helps to remove few-layered sheets, leaving single-layer MXenes in the dispersion.

The second method was the synthesis of $Ti_3C_2T_x$ by LiF + HCl etching according to a previously reported procedure.[43,44] The MAX phase Ti_3AlC_2 precursor (Carbon®, Ukraine) was first etched with a mixture of LiF (98% Sigma Aldrich) and HCl (37% Sigma Aldrich) for 22 h at 40 °C using a molar ratio of 1 : 5 between the initial MAX phase and LiF. The next washing steps were identical to ones described in the previous method.

X-ray photoelectron spectra (XPS) were recorded with a Kratos Axis Ultra electron spectrometer equipped with a delay line detector. A monochromated Al Kα source operated at 150 W, a hybrid lens system with a magnetic lens, providing an analysis area of 0.3 × 0.7 mm, and a charge neutralizer were used for the measurements. All spectra were processed with the Kratos software.[45]

Thermogravimetric analysis (TGA) curves were recorded using a Mettler Toledo TGA/DSC1 STARe system. Experiments were performed from room temperature up to 700 °C at a heating rate of 5 °C min^{-1} under nitrogen flow (50 mL min^{1}).

A Panalytical X'pert X-ray diffractometer in reflection mode with CuKα radiation was used to record part of the data for the characterization of powder samples and powder samples immersed in excess of several solvents. A thin polyethylene foil

Paper

Nanoscale

was used as a cover to prevent solvents from evaporating. Typically, a pattern was recorded in an angle range from 3.5° to 50° with a step size of 0.007°, a time per step of 65 s, and a total of 32 min per scan. The patterns were recorded a few minutes after sample preparation and the addition of solvent. For some samples repeated patterns were recorded to make sure that swelling is saturated and does not increase over time.

Experiments with heating and cooling were performed at the Rossendorf Beamline (BM20) of the European synchrotron radiation facility (ESRF),[46] using a CyroStream 800 system (Oxford Cryosystems) and radiation wavelength $\lambda = 0.7381$ Å. The MXene powder was loaded into 0.7–1 mm capillaries with excess liquid solvent and sealed to prevent solvent evaporation. Experimental data were collected in transmission geometry using a Pilatus3 X 2M detector and extracted with Bubble software.[47] The detector geometry parameters were calibrated with PyFAI using the NIST standard LaB_6. The MXene samples showed rather different sensitivities to degradation caused by the high-brilliance synchrotron X-ray beam as verified by testing using filters, which cut the intensity by factors of 50 and 100. MXenes immersed in DMSO demonstrated no degradation with 50 filters. A slow downshift of $d(001)$ was observed for unfiltered radiation. MXenes appeared to be especially sensitive to X-ray radiation in the water-immersed state, as evidenced by the change in the sample colour and the evolution of gas bubbles in the irradiated spot. Therefore, following the stability testing, temperature-dependence experiments with water and methanol immersed MXenes were performed using the intensity of incident radiation cut by a factor of 100 to ensure the absence of degradation.

3. Results

Two types of MXene $Ti_3C_2T_x$ were studied here for swelling in several polar solvents under ambient conditions. MXenes were prepared *via* LiF + HCl (MXene 1) and HF + LiCl (MXene 2) etching. The materials were characterized using XPS, XRD and TGA shortly after synthesis (see Fig. 1 and Fig. S1–S5 in the ESI†). The characterization data are in good agreement with earlier reports, confirming the successful synthesis of materials.

The swelling of MXenes 1 and 2 was studied by XRD in several liquid solvents (Fig. 1) shortly after the synthesis. The swelling of MXenes is expected to result in the intercalation of solvent between 2D sheets with expansion of the interlayer distance. The solvent-free structure shows the ordering between individual sheets in a hexagonal structure with interlayer distances of 12.4 Å and 12.9 Å for MXene 2 and MXene 1, respectively. Adding solvents results in the immediate saturation of the swelling state within several minutes required to start the measurement. Both MXenes showed almost the same increase in interlayer distance in the water-immersed state, by 3.8 Å and by 4.0 Å for MXene 2 and MXene 1, respectively. The increase is clearly larger compared with the expected thickness of one water layer (~2.5–3 Å) but smaller than the thickness of two water layers, suggesting the presence of interstratification. The swelling in water was found to be reversible; the pristine phase recovers after exposing the sample to air and water evaporation. Swelling is almost absent in acetonitrile with the increase in the d-spacing by only 1.0 Å and 0.6 Å for MXene 1 and MXene 2, respectively. Once again, random interstratification is the most common explanation for the changes in the interlayer distance of hydrophilic layered materials, which are smaller compared with the size of the solvent molecules.[48]

Note that typically swelling results in the disappearance of ordering between MXene layers. Some ordering might remain in water-swollen LiCl + HF MXenes after careful etching according to some reports but more as an exception than a rule. Therefore, the XRD reflection, which corresponds to the interlayer distance of the swollen disordered phase, should be indexed as (001) rather than (002). The $d(001)$ value directly corresponds to the interlayer distance in the MXene structure.
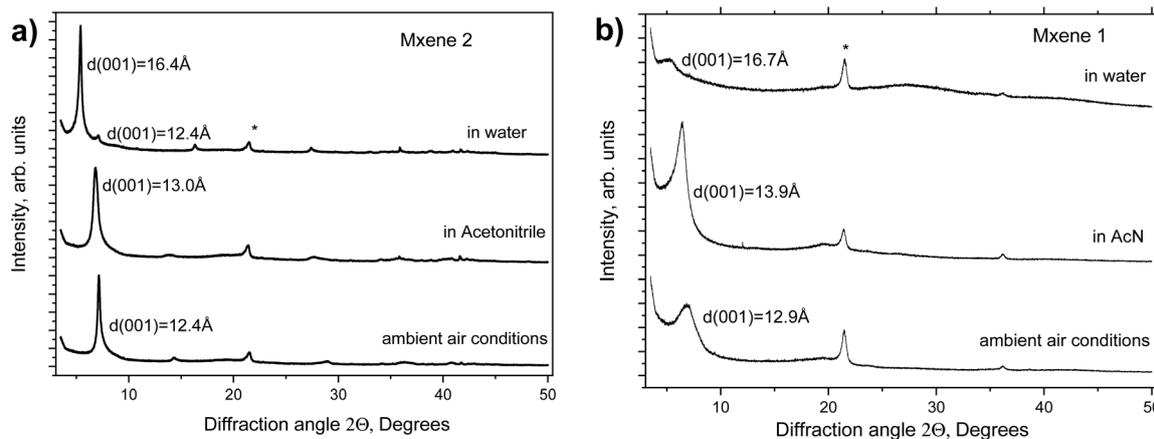

Fig. 1 XRD patterns recorded for MXenes prepared using HF + LiCl (MXene 2) (a) and LiF + HCl (MXene 1) (b) under ambient air conditions and immersed in liquid acetonitrile and water (CuKα radiation). The peak marked with * is from the plastic cover foil used to prevent solvents from evaporating.

Swelling does not result in structural changes to the 2D sheets of MXenes, changing only the distance between the layers due to the intercalation of solvents. Therefore, mostly the low-angle region of XRD patterns exhibiting a 00ℓ set of reflections will be discussed below.

The increase in the interlayer distance is in good agreement with the thickness of one methanol layer. However, the swelling of MXene 2 in ethanol was only partial with the (002) reflection of the pristine phase still present and the reflection from the swollen phase with $d(001) = 14.6$ Å.

The relative intensity of reflections from pristine and swollen phases did not change over time and was not related to the kinetic effects within 1 hour after immersion. Almost no swelling was observed for MXene 2 in larger primary alcohols: propanol, butanol and pentanol. A progressively weaker shoulder at 13.8 Å was the only trace of some swelling effect, most likely reflecting random interstratification of swollen and non-swollen layers. Almost no swelling of MXene 1 was found in all the tested alcohols except for methanol.

Summarizing the results presented in Fig. 1 and 2, the swelling of MXene 1 and MXene 2 is, in general, rather similar. Both MXenes showed good swelling in water and methanol, no swelling in acetonitrile and very poor or completely absent swelling in longer chain alcohols. This is in strong contrast to the swelling of GO, which shows strong swelling even in much longer chain alcohols (at least up to carbon number 20). The difference in swelling properties could be explained at the qualitative level by taking into account that the 2D sheets of MXenes are thicker and a lot heavier compared with GO sheets. Therefore, a lot of stronger hydration forces and swelling pressures[49] are required to move apart MXene layers. Alcohols are polar solvents due to the presence of the –OH group. However, the alkyl chain is hydrophobic and the longer the chain is, the less polar is the alcohol as a solvent.

It has to be noted that the swelling is a very sensitive indicator for the degradation of MXenes. The swelling becomes weaker with time if the samples are stored in air and even after storage in vials tightly closed under argon. The samples analyzed several weeks after synthesis no longer demonstrate the same swelling as freshly prepared materials.

A temperature-dependence study was performed using synchrotron radiation XRD using samples of MXene powder loaded into glass capillaries with an excess amount of solvent. The capillaries were sealed to prevent the evaporation of the solvent and studied using transmission geometry. A new batch of MXene 1 was prepared about 2 weeks prior to these experiments. MXene 1 appeared to be more stable to brief exposure to air in the process of loading into capillaries. The major part of the sample showed good swelling in methanol with $d(001) = 17.6$ Å at 300 K and much weaker reflection from the non-swelling part with $d(001) = 14.1$ Å.

The temperature-dependent XRD of MXene 1 immersed in methanol did not reveal phase transitions in a temperature interval range of 172–333 K (Fig. 3).

A slight decrease in the $d(001)$ of the swollen phase was observed upon cooling ($d(001) = 17.3$ Å at 172 K). This is in strong contrast to the earlier reported temperature-dependent swelling of graphite oxides, which showed either a phase transition between 1-layer and 2-layer solvate structures (for BGO)[14] or a very strong increase in the interlayer distance (for HGO)[15] upon cooling to the freezing point of methanol. No change in the structure was also observed for MXene 1 immersed in DMSO upon cooling. This is in agreement with an earlier study of an MXene–DMSO system using neutron scattering, which did not reveal anomalies below room temperature down to 20 K.[50]

However, a step-like change in the $d(001)$ value due to the swelling transition was found for MXene 1 in DMSO at temperatures above ambient (Fig. 4a). MXene 1 immersed in DMSO showed a 00ℓ set of narrow reflections from (001) to (007) with
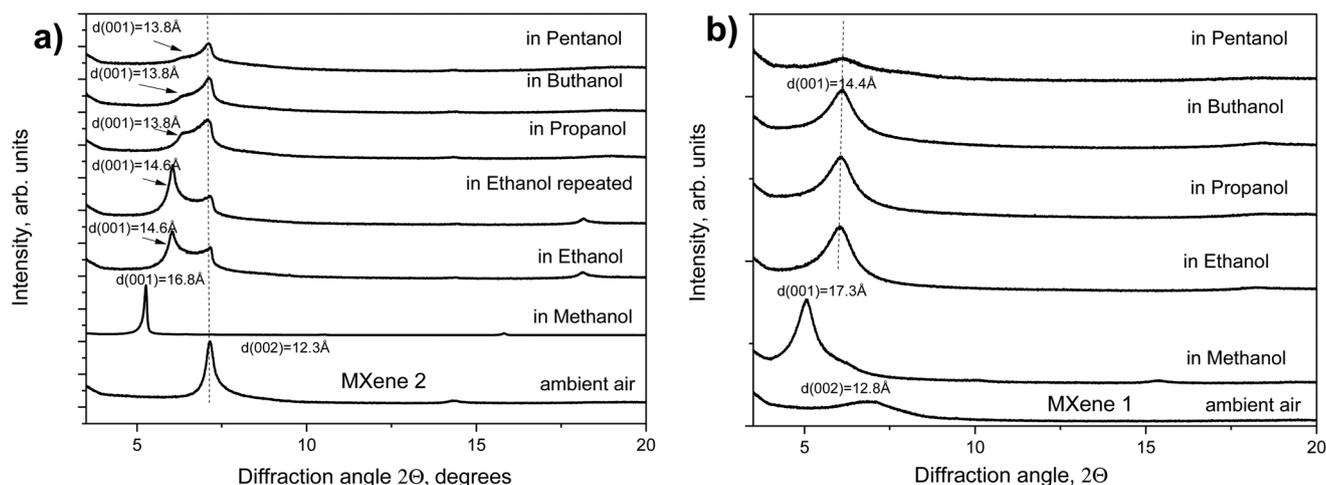

Fig. 2 XRD patterns recorded for MXenes prepared using HF + LiCl (MXene 2) (a) and LiF + HCl (MXene 1) (b) under ambient air conditions and immersed in liquid alcohols (CuKα radiation). Plastic cover foil was used to prevent solvents from evaporating.
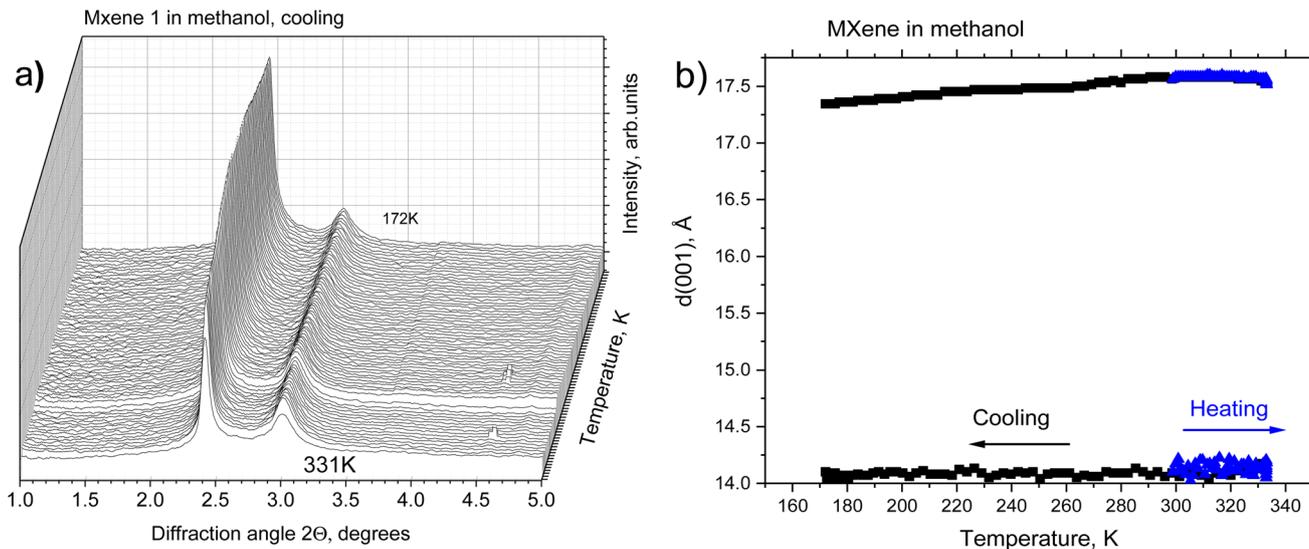
Fig. 3 Temperature-dependent swelling of MXene 1 in methanol. (a) Low-angle part of XRD patterns recorded for MXene 1 in methanol during cooling from 333 K to 172 K; λ = 0.7381 Å and (b) temperature dependence of $d(001)$ observed in the temperature cycling experiment performed by heating from ambient temperature to 333 K and cooling from 333 K to 172 K.
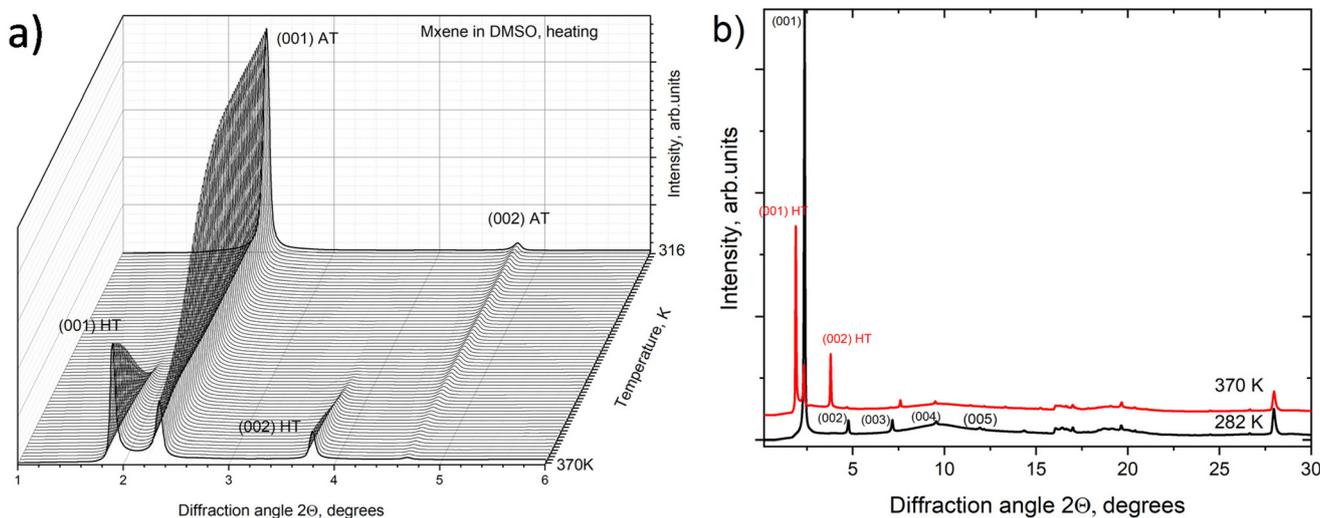

Fig. 4 (a) XRD patterns recorded for MXene 1 immersed in DMSO upon heating from ambient temperature to 370 K (part of data close to the transition temperature); only the low-angle region is shown. (b) XRD patterns recorded for MXene 1 immersed in DMSO at 282 K and 370 K. The interlayer distance of the low-temperature phase corresponds to intercalation with one layer of DMSO; the high-temperature (HT) patterns show the presence of a two-layered phase with expanded lattice.

the refined value of c-unit cell parameters (which corresponds to the interlayer distance) equal to 17.73 Å at 280 K. The diffraction pattern of MXene 1 in DMSO also shows relatively strong in-plane reflections of (010) and (110), corresponding to the a-unit cell parameter value of 3.052 Å. As noted above, no ordering of layers was observed, as evidenced by the absence of reflections, which combined h, k and ℓ indexes. Heating the MXene–DMSO sample resulted in a phase transformation. The XRD patterns recorded above 362 K showed reflections from the second set of 00ℓ reflections with an expanded c-lattice.

The XRD pattern of MXene–DMSO recorded at 370 K showed a strong reflection from the expanded phase with $d(001)$ = 22.34 Å and a weaker reflection from the ambient temperature phase with $d(001)$ = 18.10 Å (Fig. 5).

The difference of ~4.2 Å corresponded to the thickness of the DMSO layer (Fig. 4b). The incomplete transformation was likely related to the inhomogeneous structure of MXene materials with part of the layers not accessible for solvents. A similar kind of incomplete swelling transition was previously observed in a BGO–ethanol system and assigned to the
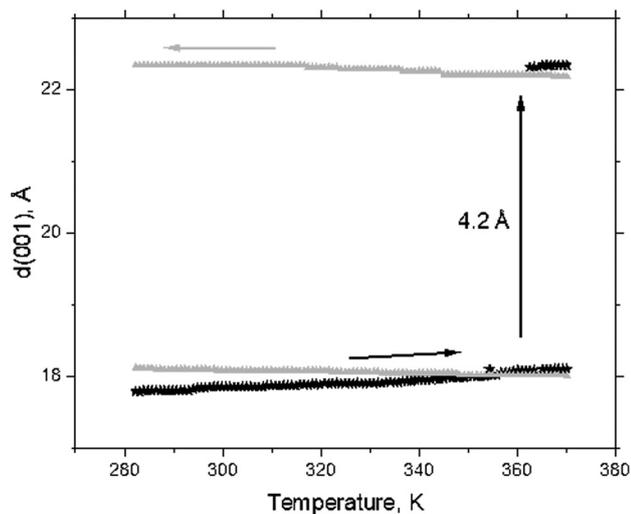
Fig. 5 Temperature dependence of the interlayer distance $d(001)$ provided for MXene 1 immersed in excess DMSO. Black symbols are for heating, and grey symbols are for the cooling parts of the temperature cycle.

inhomogeneous oxidation of graphene oxide layers.[14] Therefore, the XRD data provide evidence for the transition between the 1-layer solvate and 2-layer solvate phases in the MXene–DMSO system. Schematic structural models of these solvates are shown in Fig. 6.

To build up the theoretical models, we used the MXene structure with MXene layers terminated only by OH groups and the close-packed monolayers of DMSO cut from the crystal structure of pure DMSO.[51]

The unit cells of the intercalated structures were chosen to be commensurate with both MXene and monolayers of DMSO. The compositions of one-layer and two-layer solvates in these

models are 77 mg and 154 mg of DMSO per gram $(Ti_3C_2(OH)_2)$, respectively. The model is strongly oversimplified since the MXene layers in the real material are terminated by several kinds of functional groups and the solvent layers are completely disordered. Nevertheless, the XRD pattern-simulated models provide reasonable agreement with the experimentally observed interlayer distance in one- and two-layer solvates (Fig. S6 in the ESI†). The patterns are dominated by the high-intensity 001 reflection in both phases.

Heating and cooling experiments were also performed with a H_2O : DMSO mixture in a 2 : 1 (volume) proportion (Fig. 7). The temperature cycle started at 280 K with heating to 373 K (black symbols) followed by cooling to 173 K (green symbols) and heating back to ambient temperature (blue symbols) (Fig. 8). The $d(001) = 20.8$ Å is in good agreement with the previously reported value for MXene 1 immersed in DMSO and "hydrated" at room temperature ($d(001) = 20.2$ Å).[52]

The heating resulted in a continuous shift of the $d(001)$ peak from 20.8 Å at 280 K to 22.1 Å during the heating to 373 K. The continuous shift is typically considered as evidence of interstratification. However, splitting of the (001) reflection into two components was observed at 328 K. Simultaneously, an increase in the intensity of the (002) reflection and a sharp step-like decrease in the full width at half maximum (FWHM) of the (001) reflection occurred (see Fig. 8b). The MXene phase formed in the H_2O–DMSO mixture ($d(001) = 22.1$ Å) at high temperatures was very similar to the phase observed in the experiment with pure DMSO ($d(001 = 22.3$ Å). The data allow the following interpretation: the MXene exposed to a mixed solvent is intercalated by both water and DMSO at ambient temperature, forming randomly interstratified packing. Heating results in an increased number of layers intercalated by pure DMSO, providing a gradual shift in $d(001)$ and at temperatures above 360 K all water is expelled from the MXene
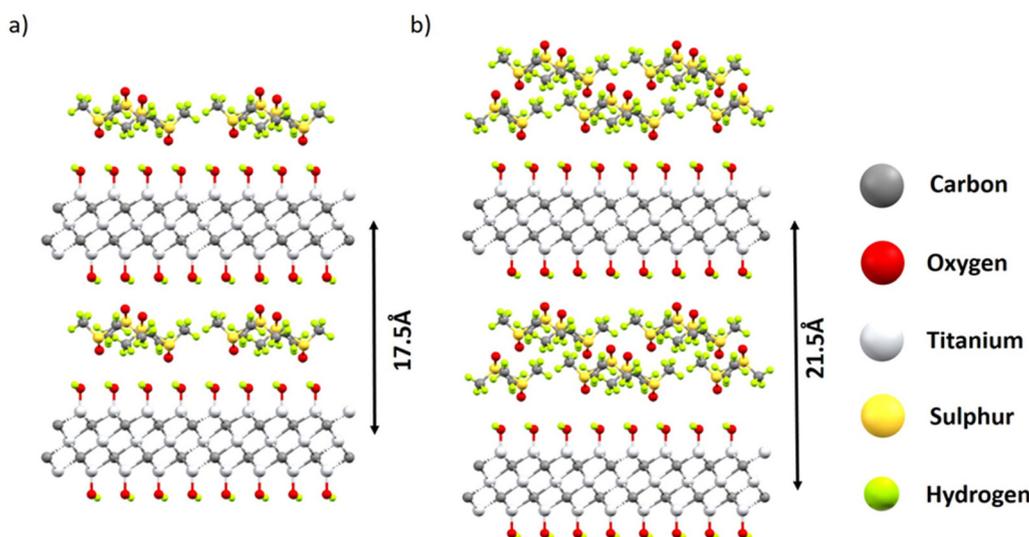

Fig. 6 A schematic structural model of MXenes intercalated with one layer of DMSO (a) and two layers of DMSO (b). The simplified model assumes that the surface of T_3C_2 layers is terminated only by OH groups.
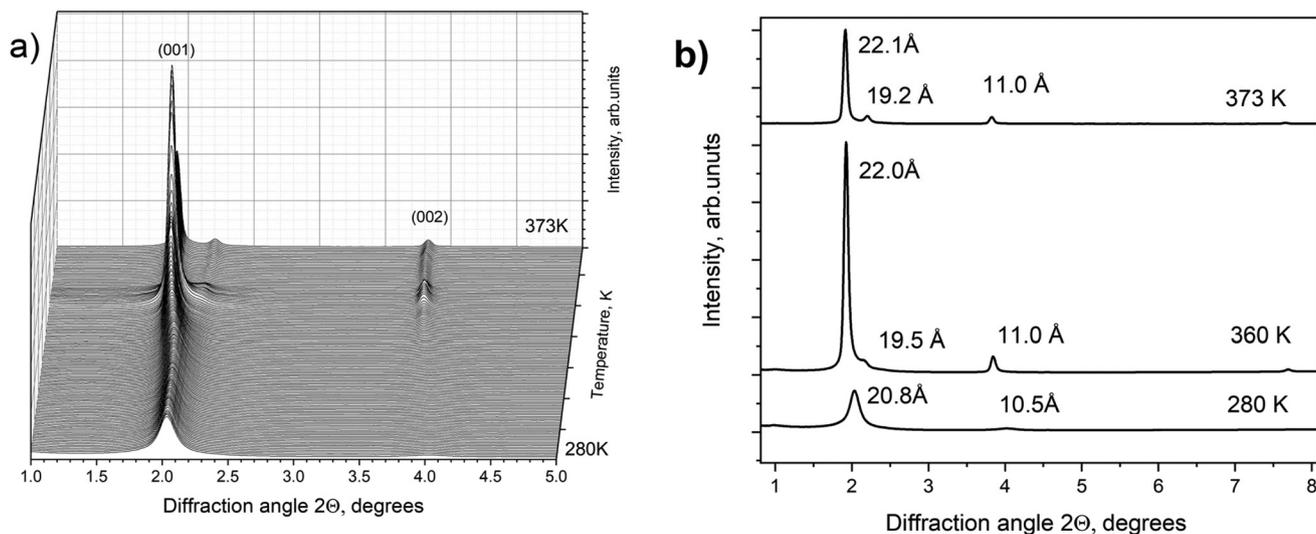
Fig. 7 (a) XRD patterns recorded for MXene 1 immersed in a 2 : 1 H$_2$O : DMSO mixture upon heating from 280 K to 373 K. The figure includes only 1/3 of the recorded patterns, showing roughly one pattern per degree. (b) XRD patterns recorded in this experiment at 280 K, 360 K and 373 K.
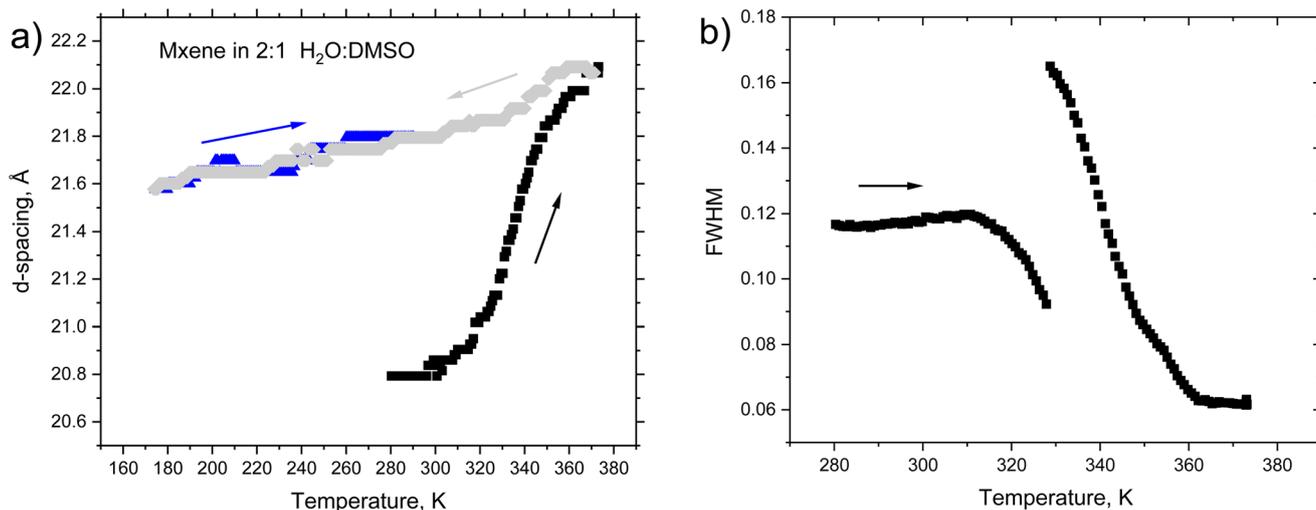

Fig. 8 (a) Temperature dependence of d(001) recorded for the sample of MXene 1 immersed in a 2 : 1 H$_2$O : DMSO mixture. The temperature cycle starts at 280 K with heating up to 373 K (black symbols) followed by cooling to 173 K (green symbols) and heating back to ambient temperature (blue symbols). (b) Temperature dependence of the FWHM of d(001) reflection.

structure. The weak reflection found at 19.2 Å (373 K) is likely to originate from a small part of the sample intercalated with one DMSO layer (as in the experiment with pure DMSO). Cooling from 373 K to 173 K followed by heating back to ambient temperature resulted only in small continuous shifts of d(001) while the high-temperature expanded phase preserved an interlayer distance of ~22 Å (Fig. S8 in the ESI†).

It is interesting to note that the phase transformation in pure DMSO occurs at a higher temperature (362 K) compared with the transition in the H$_2$O–DMSO mixture (328 K). A similar decrease in the temperature point of the swelling transition was observed previously in a GO–methanol system proportionally to the amount of added water.[53,54]

An irreversible phase transformation from the phase intercalated with one DMSO layer into two-layer DMSO–MXene has never been observed previously. There is a single report of DMSO intercalation into MXenes with the formation of a phase with d(001) = 22.4 Å available for the material produced by a different method (HF etching) after 3 weeks of storage in a desiccator.[34] However, this phase was not observed again in later studies from the same group.[50]

The phase transformation in the MXene–DMSO system is very different from transitions between one- and two-layered phases observed in BGO systems with several solvents (e.g. methanol).[14]

Phase transitions into expanded two-layered solvate phases in BGO were observed upon cooling and were completely

reversible upon heating.[14,22] The swelling transition into an expanded phase occurs in the DMSO–MXene system upon heating and is not reversible.

DMSO is very commonly used for dispersing MXenes on single sheets by sonication. However, it is usually performed at ambient temperature. The expanded phase demonstrated in our study is likely to be favourable for the delamination of bulk MXenes on single flakes. Therefore, simple heating to 370 K and cooling back to ambient temperature can be used as a preliminary step before performing sonication aimed at delamination. Moreover, it is likely that the expanded DMSO phase is more favourable for prolonged storage of MXenes after the synthesis of materials. DMSO will not only protect MXene layers from re-stacking and cross-linking reactions but also prevent the penetration of water into the interlayer space of the MXene structure. Therefore, excluding water from the structure by heating to over 328 K is likely to prolong the shelf storage time of the materials.

A possibility to change the interlayer distance of MXenes by simple temperature cycling can also be useful in membrane applications, *e.g.* when a larger interlayer distance is required for the penetration of ions and molecules in membranes. It can also be useful for the preparation of intercalated MXene structures with larger "pillaring" molecules. Our study opens up a possibility to change the size of MXene interlayers between two sharply different "pore size" states, which could also be useful in energy storage devices, allowing the penetration of larger electrolyte ions. However, one needs to note that the swelling of bulk powder materials can be significantly different compared with multi-layered membranes as previously reported for graphite oxide and GO membranes.[55]

Independently of applications, the temperature-driven transition between the intercalation of 1- and 2-layer solvents is of fundamental value for understanding swelling in hydrophilic layered materials.

We note that our study provides the first ever example of temperature-driven swelling transitions in MXenes but likely not the last considering the variety of MXene structures known at the moment[56] and the many solvents possibly inducing their swelling.

4. Conclusions

In summary, we report an irreversible swelling transition, which occurs in MXenes immersed in excess DMSO upon heating at 362–370 K with an increase in the interlayer distance by 4.2 Å. The expansion of the *c*-lattice corresponds to the thickness of one layer of DMSO and is explained by the transformation from a one-layer solvate phase at ambient temperature into a two-layered phase upon heating. Therefore, a stable expanded two-layer MXene–DMSO solvate phase can be easily produced by heating above 370 K and cooling back to room temperature. The transition temperature is lower for MXenes immersed in a 2 : 1 (by volume) H_2O : DMSO mixture. A continuous shift of $d(001)$ as a function of temperature is

observed for MXenes immersed in the mixed solvent below the transformation point (328 K). The effect of the continuous shift in the XRD peak position is explained by random inter-stratification of hydrated and DMSO solvated layers. However, water is expelled from MXene interlayers at $T > 328$ K with the formation of a pure two-layer DMSO solvate. The DMSO solvate phase preserves upon cooling back to ambient temperature in both cases when immersed in pure DMSO and DMSO mixture with water. No swelling transitions were found for MXenes immersed in DMSO/H_2O and methanol upon cooling below the freezing point of solvents. No swelling was observed in 1-alcohols longer than ethanol.

Conflicts of interest

There are no conflicts to declare.

Acknowledgements

Notes and references

1 M. Ghidiu, M. R. Lukatskaya, M. Q. Zhao, Y. Gogotsi and M. W. Barsoum, *Nature*, 2014, **516**, 78–81.

2 Z. J. Yin, Z. Lu, Y. Y. Xu, Y. H. Zhang, L. L. He, P. S. Li, L. Xiong, L. Ding, Y. Y. Wei and H. H. Wang, *Membranes*, 2021, **11**, 11080621.

3 J. Wang, Z. J. Zhang, J. N. Zhu, M. T. Tian, S. C. Zheng, F. D. Wang, X. D. Wang and L. Wang, *Nat. Commun.*, 2020, **11**, 3540.

4 J. H. Sun, A. Iakunkov, A. T. Rebrikova and A. V. Talyzin, *Nanoscale*, 2018, **10**, 21386–21395.

5 S. D. Wang, F. K. Wang, Y. Jin, X. X. Meng, B. Meng, N. A. Yang, J. Sunarso and S. M. Liu, *J. Membr. Sci.*, 2021, **638**, 119697.

6 A. Klechikov, S. You, L. Lackner, J. Sun, A. Iakunkov, A. Rebrikova, M. Korobov, I. Baburin, G. Seifert and A. V. Talyzin, *Carbon*, 2018, **140**, 157–163.

7 A. Iakunkov, J. H. Sun, A. Rebrikova, M. Korobov, A. Klechikov, A. Vorobiev, N. Boulanger and A. V. Talyzin, *J. Mater. Chem. A*, 2019, **7**, 11331–11337.

8 A. Lerf, A. Buchsteiner, J. Pieper, S. Schottl, I. Dekany, T. Szabo and H. P. Boehm, *J. Phys. Chem. Solids*, 2006, **67**, 1106–1110.

9 T. Szabo, O. Berkesi, P. Forgo, K. Josepovits, Y. Sanakis, D. Petridis and I. Dekany, *Chem. Mater.*, 2006, **18**, 2740–2749.

10 S. J. You, D. Kunz, M. Stoeter, H. Kalo, B. Putz, J. Breu and A. V. Talyzin, *Angew. Chem., Int. Ed.*, 2013, **52**, 3891–3895.

11 A. V. Talyzin, V. L. Solozhenko, O. O. Kurakevych, T. Szabo, I. Dekany, A. Kurnosov and V. Dmitriev, *Angew. Chem., Int. Ed.*, 2008, **47**, 8268–8271.

12 A. V. Talyzin, B. Sundqvist, T. Szabo, I. Dekany and V. Dmitriev, *J. Am. Chem. Soc.*, 2009, **131**, 18445–18449.

13 A. V. Talyzin, S. M. Luzan, T. Szabo, D. Chernyshev and V. Dmitriev, *Carbon*, 2011, **49**, 1894–1899.

14 S. J. You, S. Luzan, J. C. Yu, B. Sundqvist and A. V. Talyzin, *J. Phys. Chem. Lett.*, 2012, **3**, 812–817.

15 S. J. You, B. Sundqvist and A. V. Talyzin, *ACS Nano*, 2013, **7**, 1395–1399.

16 E. L. Hansen, H. Hemmen, D. M. Fonseca, C. Coutant, K. D. Knudsen, T. S. Plivelic, D. Bonn and J. O. Fossum, *Sci. Rep.*, 2012, **2**, 618.

17 A. Klechikov, J. H. Sun, I. A. Baburin, G. Seifert, A. T. Rebrikova, N. V. Avramenko, M. V. Korobov and A. V. Talyzin, *Nanoscale*, 2017, **9**, 6929–6936.

18 C. Cabrillo, F. Barroso-Bujans, R. Fernandez-Perea, F. Fernandez-Alonso, D. Bowron and F. J. Bermejo, *Carbon*, 2016, **100**, 546–555.

19 A. Iakunkov and A. V. Talyzin, *Nanoscale*, 2020, **12**, 21060–21093.

20 A. V. Talyzin, G. Mercier, A. Klechikov, M. Hedenstrom, D. Johnels, D. Wei, D. Cotton, A. Opitz and E. Moons, *Carbon*, 2017, **115**, 430–440.

21 S. J. You, S. M. Luzan, T. Szabo and A. V. Talyzin, *Carbon*, 2013, **52**, 171–180.

22 A. V. Talyzin, A. Klechikov, M. Korobov, A. T. Rebrikova, N. V. Avramenko, M. F. Gholami, N. Severin and J. P. Rabe, *Nanoscale*, 2015, **7**, 12625–12630.

23 A. T. Rebrikova, A. Klechikov, A. Iakunkov, J. H. Sun, A. V. Talyzin, N. V. Avramenko and M. Korobov, *J. Phys. Chem. C*, 2020, **124**, 23410–23418.

24 A. V. Talyzin and S. M. Luzan, *J. Phys. Chem. C*, 2010, **114**, 7004–7006.

25 A. V. Talyzin, B. Sundqvist, T. Szabo and V. Dmitriev, *J. Phys. Chem. Lett.*, 2011, **2**, 309–313.

26 B. Rezania, N. Severin, A. V. Talyzin and J. P. Rabe, *Nano Lett.*, 2014, **14**, 3993–3998.

27 C. A. Voigt, M. Ghidiu, V. Natu and M. W. Barsoum, *J. Phys. Chem. C*, 2018, **122**, 23172–23179.

28 E. S. Muckley, M. Naguib, H. W. Wang, L. Vlcek, N. C. Osti, R. L. Sacci, X. H. Sang, R. R. Unocic, Y. Xie, M. Tyagi, E. Mamontov, K. L. Page, P. R. C. Kent, J. Nanda and I. N. Ivanov, *ACS Nano*, 2017, **11**, 11118–11126.

29 L. Verger, V. Natu, M. Ghidiu and M. W. Barsoum, *J. Phys. Chem. C*, 2019, **123**, 20044–20050.

30 Y. J. Zhang, Y. D. Jiang, Z. H. Duan, Q. Huang, Y. W. Wu, B. H. Liu, Q. N. Zhao, S. Wang, Z. Yuan and H. L. Tai, *Sens. Actuators, B*, 2021, **344**, 130295.

31 M. Ghidiu, S. Kota, V. Drozd and M. W. Barsoum, *Sci. Adv.*, 2018, **4**, eaao685.

32 M. Naguib, R. R. Unocic, B. L. Armstrong and J. Nanda, *Dalton Trans.*, 2015, **44**, 9353–9358.

33 M. Naguib, M. Kurtoglu, V. Presser, J. Lu, J. J. Niu, M. Heon, L. Hultman, Y. Gogotsi and M. W. Barsoum, *Adv. Mater.*, 2011, **23**, 4248–4253.

34 O. Mashtalir, M. Naguib, V. N. Mochalin, Y. Dall'Agnese, M. Heon, M. W. Barsoum and Y. Gogotsi, *Nat. Commun.*, 2013, **4**, 1716.

35 M. R. Lukatskaya, O. Mashtalir, C. E. Ren, Y. Dall'Agnese, P. Rozier, P. L. Taberna, M. Naguib, P. Simon, M. W. Barsoum and Y. Gogotsi, *Science*, 2013, **341**, 1502–1505.

36 M. Ghidiu, J. Halim, S. Kota, D. Bish, Y. Gogotsi and M. W. Barsourm, *Chem. Mater.*, 2016, **28**, 3507–3514.

37 S. Kajiyama, L. Szabova, K. Sodeyama, H. Iinuma, R. Morita, K. Gotoh, Y. Tateyama, M. Okubo and A. Yamada, *ACS Nano*, 2016, **10**, 3334–3341.

38 N. C. Osti, M. Naguib, K. Ganeshan, Y. K. Shin, A. Ostadhossein, A. C. T. van Duin, Y. Q. Cheng, L. L. Daemen, Y. Gogotsi, E. Mamontov and A. I. Kolesnikov, *Phys. Rev. Mater.*, 2017, **1**, 065406.

39 M. Daab, N. J. Eichstaedt, C. Habel, S. Rosenfeldt, H. Kalo, H. Schiessling, S. Forster and J. Breu, *Langmuir*, 2018, **34**, 8215–8222.

40 V. Natu, R. Pai, O. Wilson, E. Gadasu, H. Badr, A. Karmakar, A. J. D. Magenau, V. Kalra and M. W. Barsoum, *Chem. Mater.*, 2022, **34**, 678–693.

41 H. P. Boehm, A. Clauss and U. Hofmann, *J. Chim. Phys. Phys.-Chim. Biol.*, 1961, **58**, 141–147.

42 T. Szabo, E. Tombacz, E. Illes and I. Dekany, *Carbon*, 2006, **44**, 537–545.

43 K. Chen, X. Yan, J. Li, T. Jiao, C. Cai, G. Zou, R. Wang, M. Wang, L. Zhang and Q. Peng, *Nanomaterials*, 2019, **9**, 284.

44 T. Zhang, L. Pan, H. Tang, F. Du, Y. Guo, T. Qiu and J. Yang, *J. Alloys Compd.*, 2017, **695**, 818–826.

45 R. C. D. Wagner, W. M. Riggs, L. E. Davis, J. F. Moulder and G. E. Muilenberg, *Handbook of X-ray Photoelectron Spectroscopy*, Perkin-Elmer, Co., Minnesota, 1979.

46 A. C. Scheinost, J. Claussner, J. Exner, M. Feig, S. Findeisen, C. Hennig, K. O. Kvashnina, D. Naudet, D. Prieur, A. Rossberg, M. Schmidt, C. R. Qiu, P. Colomp, C. Cohen, E. Dettona, V. Dyadkin and T. Stumpf, *J. Synchrotron Radiat.*, 2021, **28**, 333–349.

47 V. Dyadkin, P. Pattison, V. Dmitriev and D. Chernyshov, *J. Synchrotron Radiat.*, 2016, **23**, 825–829.

48 S. Celerier, S. Hurand, C. Garnero, S. Morisset, M. Benchakar, A. Habrioux, P. Chartier, V. Mauchamp, N. Findling, B. Lanson and E. Ferrage, *Chem. Mater.*, 2019, **31**, 454–461.

49 A. Iakunkov, N. Boulanger, A. Nordenstrom and A. V. Talyzin, *Adv. Mater. Interfaces*, 2021, **8**, 2100552.

50 X. Wang, T. S. Mathis, K. Li, Z. Lin, L. Vlcek, T. Torita, N. C. Osti, C. Hatter, P. Urbankowski, A. Sarycheva, M. Tyagi, E. Mamontov, P. Simon and Y. Gogotsi, *Nat. Energy*, 2019, **4**, 241–248.

51 H. Reuter, *Acta Crystallogr., Sect. E: Crystallogr. Commun.*, 2017, **73**, 1405–1408.

52 L. Wang, W. Q. Tao, L. Y. Yuan, Z. R. Liu, Q. Huang, Z. F. Chai, J. K. Gibson and W. Q. Shi, *Chem. Commun.*, 2017, **53**, 12084–12087.

53 S. J. You, J. C. Yu, B. Sundqvist, L. A. Belyaeva, N. V. Avramenko, M. V. Korobov and A. V. Talyzin, *J. Phys. Chem. C*, 2013, **117**, 1963–1968.

54 S. J. You, J. C. Yu, B. Sundqvist and A. V. Talyzin, *Phys. Status Solidi B*, 2012, **249**, 2568–2571.

55 A. V. Talyzin, T. Hausmaninger, S. J. You and T. Szabo, *Nanoscale*, 2014, **6**, 272–281.

56 Y. Gogotsi and B. Anasori, *ACS Nano*, 2019, **13**, 8491–8494.